

Article

Electrodeposited PPy@TiO₂ and PEDOT@TiO₂ Counter Electrodes for [Co(bpy)₃]^{2+/3+} Redox Mediator-Based Dye-Sensitized Solar Cells

Abdelaal S. A. Ahmed ^{1,*} , Xie Yi ², Xiujuan Zhao ^{2,*}, Wanchun Xiang ^{2,3} and Mohammed Abdelmotallieb ¹¹ Chemistry Department, Faculty of Science, Al-Azhar University, Assiut 71524, Egypt² State Key Laboratory of Silicate Materials for Architecture, Wuhan University of Technology, Luoshi Road, Wuhan 430070, China³ Key Laboratory for Applied Surface and Colloid Chemistry, Ministry of Education, Shaanxi Key Laboratory for Advanced Energy Devices, Shaanxi Engineering Lab for Advanced Energy Technology, School of Materials Science & Engineering, Shaanxi Normal University, Xi'an 710119, China

* Correspondence: abdelaalsaiyd@gmail.com or abdelaalsaiyd@azhar.edu.eg (A.S.A.A.); opluse@whut.edu.cn (X.Z.); Tel.: +20-1553681043 (A.S.A.A.)

Abstract: The main goal of this work is to enhance the catalytic performance of PPy and PEDOT films toward the Co²⁺/Co³⁺ redox couple. PPy and PEDOT films were electrodeposited separately on a porous TiO₂ template to assess their suitability as alternative catalysts in dye-sensitized solar cells (DSSC) based on the [Co(bpy)₃]^{2+/3+} redox shuttle. The obtained PPy@TiO₂ and PEDOT@TiO₂ counter electrodes displayed much rougher surfaces. Electrochemical studies indicate the superior catalytic activity of both the electrodeposited electrodes toward Co³⁺ reduction, as indicated by lower charge transfer resistance than that of pristine films and even that of Pt electrodes. Therefore, the fabricated DSSC devices with these counter electrodes achieved higher power conversion efficiencies compared to cells with pristine PPy and PEDOT counter electrodes, or even with a Pt counter electrode. Interestingly, the assembled DSSC device with a PEDOT@TiO₂ counter electrode displayed the highest performance among all with a power conversion efficiency of 6.62%, which is better than that obtained by the device with a Pt electrode (6.07%).

Keywords: dye-sensitized solar cells; counter electrodes; copper polypyridyl redox shuttle; conductive polymers; electrochemical deposition



Citation: Ahmed, A.S.A.; Yi, X.; Zhao, X.; Xiang, W.; Abdelmotallieb, M. Electrodeposited PPy@TiO₂ and PEDOT@TiO₂ Counter Electrodes for [Co(bpy)₃]^{2+/3+} Redox Mediator-Based Dye-Sensitized Solar Cells. *Inorganics* **2022**, *10*, 213. <https://doi.org/10.3390/inorganics10110213>

Academic Editor: Catherine Housecroft

Received: 20 October 2022

Accepted: 14 November 2022

Published: 18 November 2022

Publisher's Note: MDPI stays neutral with regard to jurisdictional claims in published maps and institutional affiliations.



Copyright: © 2022 by the authors. Licensee MDPI, Basel, Switzerland. This article is an open access article distributed under the terms and conditions of the Creative Commons Attribution (CC BY) license (<https://creativecommons.org/licenses/by/4.0/>).

1. Introduction

Environmental pollution and climate change are the most prominent threats facing humanity in recent times due to the imposing and increasing use of fossil and non-renewable energy sources, so the search for safe and environmentally friendly alternative energy sources has become an urgent matter, not a luxury. In the last decades, solar energy has received great attention as one of the most encouraging sustainable energy sources for future generations due to its availability worldwide [1]. Solar cells or photovoltaics (PV) are a promising technique used to make use of solar energy by converting it to electrical energy via the photovoltaic effect [2]. Until now, various kinds of solar cells have been developed with considerable power conversion efficiency; however, the high production costs and low abundance of toxic metals restrict their wide installation. Thus, intensive efforts have been made to develop cheaper and more eco-friendly solar cells.

Since 1991, dye-sensitized solar cells (DSSCs) have attracted remarkable attention as a promising alternative to traditional silicon-based solar cells [3,4]. This is due to their simple fabrication with low-cost materials, relatively high power conversion efficiency, effective response to diffused light, and compatibility with building window glass or on a flexible substrate [4]. Due to continuous development, the conversion efficiency of the

DSSCs recently exceeds 13% under full sun illumination (AM 1.5G) [5,6]. Typically, a DSSC device is composed of a photoanode to absorb the incident sunlight, an electrolyte with a redox mediator as the inner transport medium to provide ionic conductivity, and a counter electrode (CE). The CE is the part responsible for collecting the electron from the external circuit to catalyze the reduction of the oxidized species of the redox couple; the reduced form of the redox couple will diffuse to the anode and hence regenerate the oxidized form of the dye to its ground state via photo-injection of the electrons into the porous TiO_2 film. Therefore, the CE should display a lower charge transfer electron at the CE/electrolyte interface to promote the full process. The full structure of a DSSC device and the work function process are shown in Figure 1 [7–9].

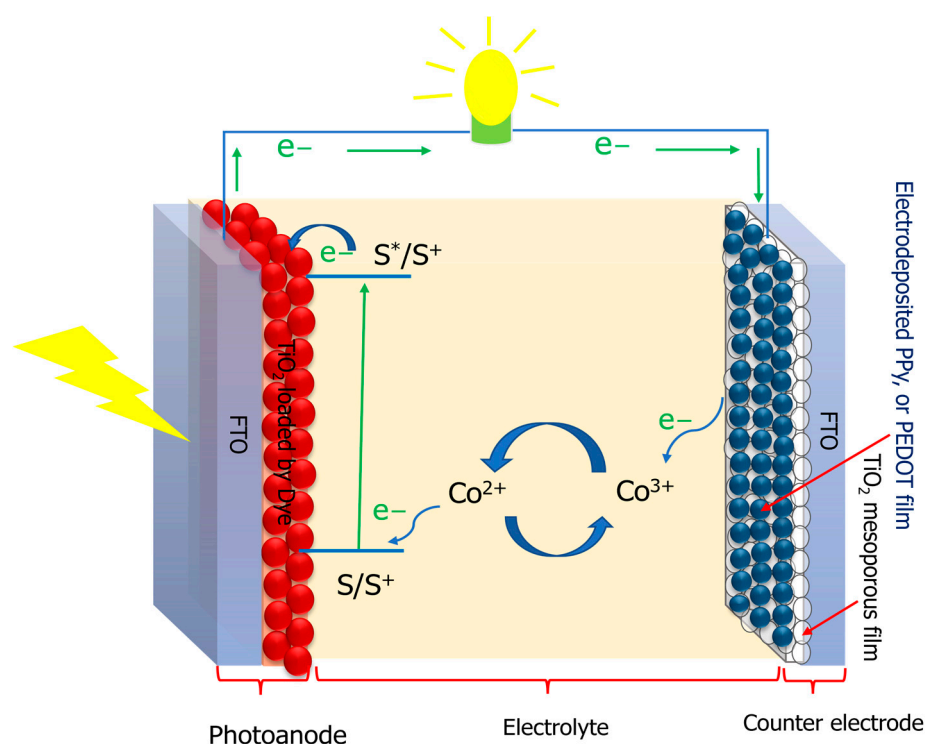


Figure 1. Schematic representation of DSSC device showing photoanode and counter electrode with an electrolyte sandwiched in the gap between them.

Conventionally, I_3^-/I^- is the most common redox system for DSSCs with high performance [10–12]. However, the I_3^-/I^- redox system has some limitations, including a relatively low redox potential (0.35 V), a low open circuit voltage (V_{OC}), and a short circuit current density (J_{SC}), as well as a corrosive nature toward metallic grids. Moreover, the I_3^-/I^- redox shuttle shows partial absorption in visible light ($\lambda \sim 300\text{--}430\text{ nm}$) due to the presence of the triiodide (I_3^-) species [13]. Therefore, various alternative redox couples such as nickel(III/IV) [14], copper(I/II) [15], disulfide/thiolate (T_2/T^-) [16], ferrocene/ferrocenium (Fc/Fc^+) [17], and $\text{Co}^{2+}/\text{Co}^{3+}$ [18] have been developed in order to overcome these limitations. Cobalt-based complexes have received great attention as promising alternative redox couples, this is due to various advantages such as non-corrosive toward metallic cathodes, non-volatility, lightly colored and tunable redox potentials by modification of the attached ligands [18–23]. Recently, Co(II/III) -polypyridyl complexes ($[\text{Co}(\text{bpy})_3]^{2+/3+}$; bpy = 2, 2'-bipyridine) have attracted intensive interest as a redox couple in DSSCs with higher power conversion efficiency (PCE). For example, Yella et al. reported that the assembled devices in conjunction with the $[\text{Co}(\text{bpy})_3]^{2+/3+}$ redox couple and donor- π -bridge-acceptor porphyrin sensitizer (YD2-o-C8) showed PCE of 12.3% [24]. Further enhancement was achieved by the incorporation of a proquinoidal benzothiadiazole (BTD) into the porphyrin structure. The DSSC demonstrated a PCE of 13% [5]. However, the

$\text{Co}^{2+}/\text{Co}^{3+}$ complex system is a one-electron transfer that displays fast recombination of electrons from the CB of the TiO_2 [25]. In addition, the larger molecular size of the $\text{Co}^{2+}/\text{Co}^{3+}$ complexes limits their mass diffusion in the electrolyte solution and the porous semiconductor [26,27]. Typically, organic dyes with high extinction coefficients allow using thinner TiO_2 films, as well as highly catalytic CEs to quickly reduce Co^{3+} to Co^{2+} to overcome the diffusion issue and decrease the recombination reaction rate to achieve high conversion efficiency [27,28].

Although Pt-CE is the most widely used catalytic material for the I_3^-/I^- redox system with high catalytic performance, the high cost, corrosion ability in the presence of the iodide-based electrolyte, and the high temperature needed for preparing the Pt CE are the main challenges that need to be solved. Thus, various catalytic materials have been developed and utilized as alternative CEs without sacrificing catalytic activity. For example, Zhang et al. [29] significantly enhanced the catalytic performance of Kesterite $\text{Cu}_2\text{ZnSnS}_4$ (CZTS) toward I_3^- reduction via the element substitution of Zn^{2+} by Co^{2+} and Ni^{2+} cations. The assembled DSSC with modified CZTS showed a PCE of 8.3%, which is comparable with that achieved with the Pt CE. Furthermore, binary metal sulfides ($\text{Cu}_x\text{Co}_y\text{S}_z$) displayed a potential ability as an alternative CE for DSSCs with the I_3^-/I^- redox couple, as indicated by a higher PCE (8.60%), which is better than that achieved with Pt-CE (7.75%) [25]. Metal selenides also showed potential catalytic activity as reported by Ho et al., in which a hierarchical urchin-like structure of $\text{CoSe}_2/\text{CoSeO}_3$ was synthesized via the one-step hydrothermal method [30]. The electrochemical analysis showed that the PCE of the related assembled DSSCs is 9.29%, which is better than that of the cell with Pt CE (8.33%). Furthermore, under 2.21 mW cm^{-2} light intensity, the devices with the $\text{CoSe}_2/\text{CoSeO}_3$ CE had a PCE of 19.88%. This indicates that $\text{CoSe}_2/\text{CoSeO}_3$ CE is a promising alternative CE for DSSCs under outdoor and indoor conditions. Carbon-based materials also showed outstanding catalytic performance toward the I_3^-/I^- redox couple. For example, Pang et al. reported that the nitrogen-doped carbon nano-onions with modified reduced graphene (N-CNOs/mGr) composite displayed higher and excellent catalytic activity toward I_3^- reduction, and even better than that achieved with the standard Pt CE. The PCE of the related liquid state DSSC with N-CNOs/mGr was 10.28%, which is much higher than that of the Pt CE (6.54%) [31]. In the last few years, our group utilized carbon-based materials such as NiO@C-derived from walnut shell [32], carbon black- Si_3N_4 [33], and carbon black- SiO_2 as alternative CEs with promising catalytic performances [34]. However, for the monoelectronic redox couples based on coordination compounds such as the $\text{Co}^{2+}/\text{Co}^{3+}$ system, Pt is not the best catalytic material [35]. For example, Kavan et al. reported that the electrocatalytic performance of the graphene nanoplatelets (GNP) coated on fluorine-doped SnO_2 (FTO) is higher than that achieved with the Pt CE. The PCE of the assembled DSSCs with GNP is superior to that with the Pt CE under the same working conditions [36]. Furthermore, Ju et al. [37], reported that the DSSC with electro-spray nitrogen-doped graphene nanoplatelets (NGnP) CE showed a PCE of 9.05%, which is superior to that with the Pt CE (8.43%). According to Lee et al., carbon black (CB) demonstrated promising catalytic performance toward the $[\text{Co}(\text{bpy})_3]^{2+/3+}$ redox mediator [38]. The assembled DSSCs exhibited a PCE of 8.81%, which is much better than that of the Pt CE (7.10%). Recently, Han et al. [39], prepared $\text{Cu}_{2-x}\text{Se@N}$ -doped carbon nanosheets as transparent CE by using a Cu-TCPP metal-organic framework thin film as a template in the presence of selenium powder under a nitrogen atmosphere. The bifacial DSSCs fabricated achieved a PCE of 7.61% and 5.82% from the front and rear irradiation, respectively, which is comparable to that with Pt CE.

Conducting polymers often outperformed Pt CEs in electrocatalytic activities toward the $[\text{Co}(\text{bpy})_3]^{2+/3+}$ redox couple. The most efficient PEDOT-based CEs are prepared by electrodeposition methods [40]. For instance, Bignozzi et al. demonstrated that electrodeposited poly(3,4-ethylenedioxythiophene) (PEDOT) CE has distinct electrocatalytic activity toward $[\text{Co}(\text{bpy})_3]^{2+/3+}$ redox mediators, and the total performance of the assembled DSSCs is competitive with that for Au and Pt CEs [28]. Doping is an efficient technique for

enhancing the catalytic performance of the PEDOT-based CEs. For example, Boschloo et al. revealed that the electrocatalytic performance of the PEDOT doped with iron (III) tris-p-toluenesulfonate (PEDOT: Tos) toward the $[\text{Co}(\text{bpy})_3]^{2+/3+}$ redox shuttle exceeded that of the Pt CE. The DSSCs with PEDOT: Tos CE yielded a PCE of 6.3%, higher than with the Pt CE (6.1%) [41]. Utilizing sodium dodecyl sulfate (SDS) or LiClO_4 are the famous dopants for PEDOT, in which the SDS is performed in water solution and the latter in organic media. SDS in water is preferred due to the non-flammability, low cost and abundance of water. In addition, it is more suitable for large-scale production. Most recently, Carli et al. [35], reported that the electrocatalytic activity of the electrodeposited PEDOT/Nafion toward a $\text{Co}^{2+}/\text{Co}^{3+}$ -based redox mediator was comparable to that of PEDOT/ ClO_4 and significantly superior to that of PEDOT/PSS. The electrodeposited doped PEDOT showed superior catalytic activity toward the $\text{Co}^{2+}/\text{Co}^{3+}$ -based redox mediators. However, the total performance still needs extensive work to be suitable for market production.

Poly pyrrole (PPy) is another conducting polymer that has attracted intensive attention as a promising alternative CE due to its high conductivity, low cost, as well as considerable electrocatalytic activity for I_3^- reduction. Although several studies have reported the successful use of PPy as a CE for redox-based DSSCs [40–42], its applications in Cobalt-based devices are still uncommon. Although the promising performance of both PEDOT and PPy as alternative CEs toward the $\text{Co}^{2+}/\text{Co}^{3+}$ -based redox mediators, the smooth surface morphology is a challenge, which sacrifices the performance of the assembled DSSC devices. Inserting a 3D porous template between the substrate and the electrodeposited film showed a promising strategy for enhancing the electrocatalytic performance. For example, Cheng et al. reported that inserting TiC or TiN nanoparticles as 3D porous templates remarkably enhanced the catalytic performance of the electrodeposited PEDOT toward the $\text{Co}^{2+}/\text{Co}^{3+}$ -polypyridyl redox mediator compared with pristine PEDOT CE or even with Pt CE [27]. In this work, a screen-printed TiO_2 film was utilized as a porous template for the electrodeposited PPy, and PEDOT layers. The morphology and electrochemical properties of PEDOT@ TiO_2 and PPy@ TiO_2 CEs, as well as their use as Pt-free catalysts for the $[\text{Co}(\text{bpy})_3]^{2+/3+}$ redox couple, are discussed. To the best of our knowledge, this is the first time such CEs have been used for DSSCs based on a $\text{Co}^{2+}/\text{Co}^{3+}$ mediator. This has revealed the potential ability to utilize PEDOT@ TiO_2 and PPy@ TiO_2 as alternative CEs in DSSCs.

2. Results and Discussion

2.1. Morphological Analysis of the Electrodeposited CEs

The purpose of this work is to provide a porous template for the PEDOT and PPy films to increase the exposed surface area for the electrolyte, which is preferred for catalytic activity, and thus improve the total performance of the assembled DSSCs. The surface morphologies of the electrodeposited CEs (PPy, PEDOT, PPy@ TiO_2 , and PEDOT@ TiO_2) were studied by FE-SEM; the images obtained are shown in Figure 2. The morphology of the electrodeposited PPy film in Figure 2a reveals a highly compact spherical-like dense structure. Despite the PEDOT film (Figure 2c) showing a porous and spherical-like structure, the deposited film appears to be disorderly coated on the FTO substrate. Such morphologies (compact, and disordered) are unfavorable for the catalytic activity as they limit the electron transfer and thus reduce the total photovoltaic performance of the assembled DSSCs. Compared with pristine PPy, and PEDOT films, the PPy@ TiO_2 and PEDOT@ TiO_2 (Figure 2b,d) display rougher, porous structures, revealing a higher electrochemical surface area available for reduction reactions, which is crucial for the photovoltaic performance of the DSSCs.

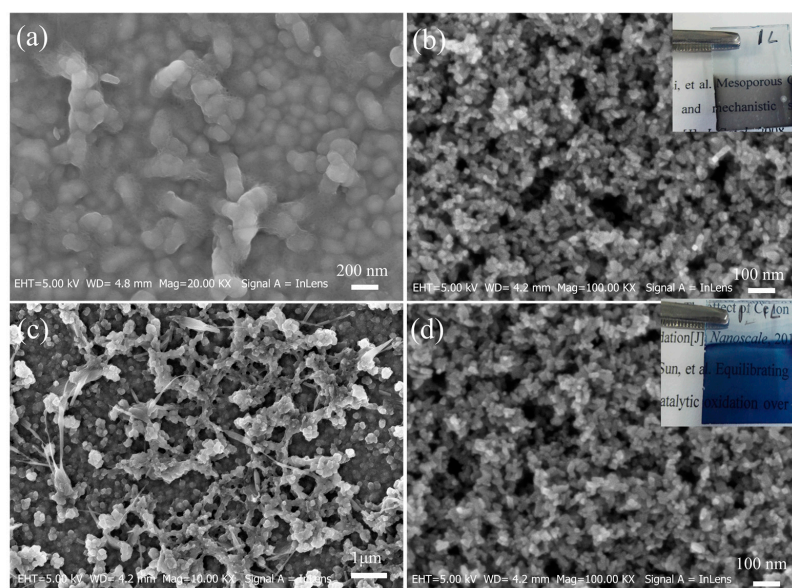


Figure 2. SEM images of (a) PPy film, (b) PPy@TiO₂ film, (c) PEDOT film, and (d) PEDOT@TiO₂ film (the inserted images in b, d are the photographs of PPy@TiO₂ and PEDOT@TiO₂ films, respectively).

SEM cross-section images of the four electrodeposited films (PPy, PEDOT, PPy@TiO₂, and PEDOT@TiO₂) were obtained to determine the average thickness of the electrodeposited films. In this study, all CEs were prepared under the same conditions. From the cross-section SEM images in Figure 3, all films displayed high contact with the FTO substrate, which reveals the high stability of the prepared CEs. The average thickness of the screen-printed TiO₂ is about 520 nm. The PPy (Figure 3a) and PEDOT (Figure 3c) layers displayed average thicknesses of 230 nm and 330 nm, respectively. Moreover, the electrodeposited films on the TiO₂ template displayed a much higher thickness, revealing a much rougher surface, which is highly desirable for catalytic reactions. The estimated thickness of the PPy (Figure 3b) and PEDOT (Figure 3d) coated on the TiO₂ layer are 830 nm and 850 nm, respectively.

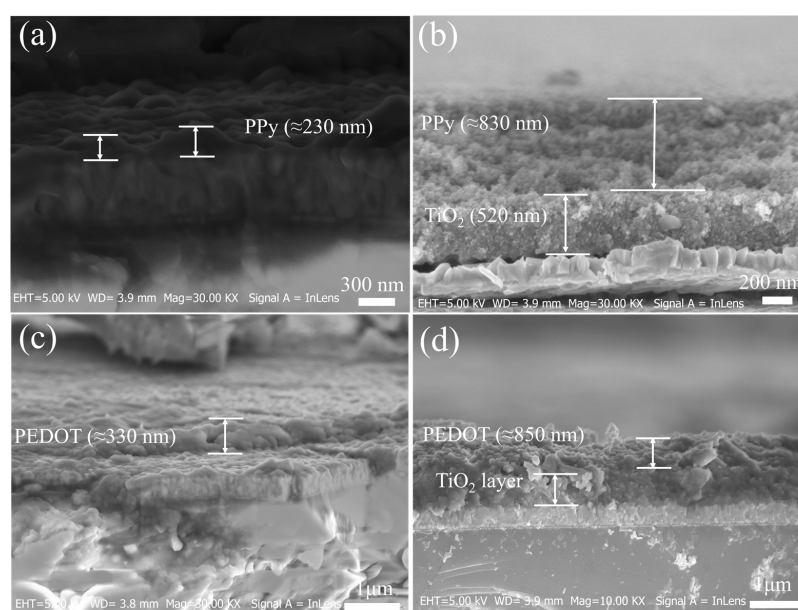


Figure 3. SEM images of cross-section of (a) PPy film (230 nm), (b) PPy@TiO₂ film, (c) PEDOT film (330 nm), and (d) PEDOT@TiO₂ film.

2.2. Electrochemical Analysis

Generally, there are various techniques for investigating the electrochemical properties of the utilized CEs, such as CV, EIS, and Tafel plots. Cyclic voltammograms (CVs) were performed to investigate the electrocatalytic performance of the different deposited electrodes in an acetonitrile solution containing the $\text{Co}^{2+}/\text{Co}^{3+}$ redox couple. A typical CV curve for the redox reaction of the $[\text{Co}(\text{bpy})_3]^{2+/3+}$ redox mediator has one redox peak due to this reaction being a one-electron transfer reaction. As shown in Figure 4a, and the related data presented in Table 1, the electrodeposited PPy and PEDOT CEs showed considerable catalytic activity toward the $\text{Co}^{2+}/\text{Co}^{3+}$ redox reaction. Furthermore, the recorded CV curves have a similar shape to that of Pt CE, indicating similar catalytic activity. In comparison with the thermally deposited Pt CE, the catalytic performance of PPy CE is lower, as evidenced by the lower peak current density (J_{PC}), while the PEDOT displayed higher catalytic activity as indicated by a larger J_{PC} ($-0.631 \text{ mA cm}^{-2}$). The potential difference between the anodic and cathodic redox peaks (ΔE_{PP}) for the PPy and the PEDOT CEs is lower than that for the Pt CE, which indicates a higher redox reaction rate [42]. As shown in Table 1, the electrocatalytic activity of the PPy and PEDOT CEs significantly enhanced after deposition onto the TiO_2 film, as indicated by increasing the J_{PC} from $-0.482 \text{ mA cm}^{-2}$ for pure PPy CE to $-0.665 \text{ mA cm}^{-2}$ for PPy@ TiO_2 CE, and from $-0.631 \text{ mA cm}^{-2}$ for pure PEDOT CE to $-0.740 \text{ mA cm}^{-2}$ for PEDOT@ TiO_2 CE. The higher current density indicates faster charge transfer at the CE surface due to the higher surface area [43,44]. As shown in Table 1, the ΔE_{PP} for all deposited CEs is lower than that for the Pt CE; however, the values of both PPy@ TiO_2 and PEDOT@ TiO_2 CEs are still higher than the pure films, this can be assigned to lower conductivity due to the presence of the semiconducting TiO_2 layer [43]. Among all CEs, the PEDOT@ TiO_2 CE displayed the best catalytic performance toward the $\text{Co}^{2+}/\text{Co}^{3+}$ redox reaction.

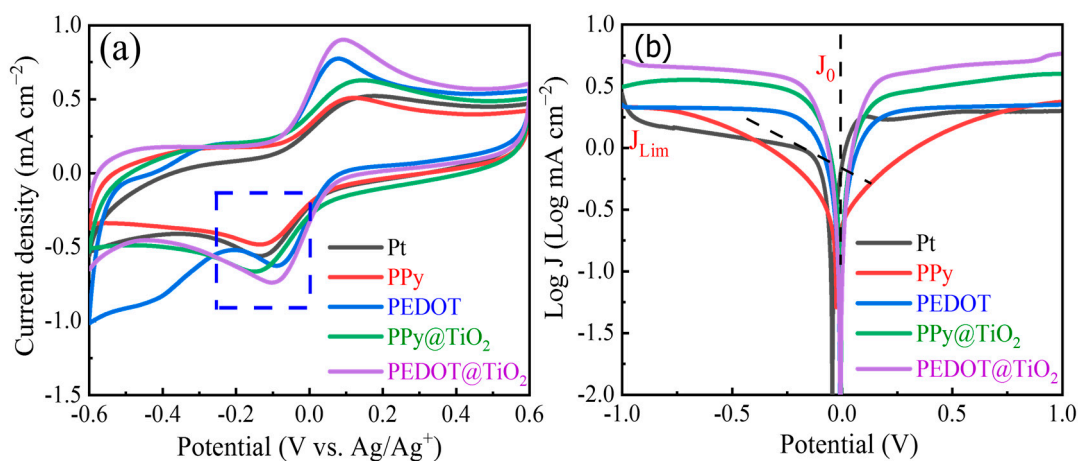


Figure 4. (a) Cyclic voltammograms for the redox reaction of $[\text{Co}(\text{bpy})_3]^{2+/3+}$ and (b) Tafel polarization plots for the symmetrical cells with Pt, PPy, PEDOT, PPy@ TiO_2 , and PEDOT@ TiO_2 CEs.

Table 1. CV, and Tafel parameters of the symmetric cells with various CEs and $[\text{Co}(\text{bpy})_3]^{2+/3+}$ redox couple.

CEs	J_{PC} (mA cm^{-2})	ΔE_{PP} (mV)	Log J_0 (mA cm^{-2})	Log J_{lim} (mA cm^{-2})	D_n ($\text{cm}^{-2} \text{ S}^{-1}$)
Pt	-0.559	0.319	-0.117	0.435	5.88×10^{-7}
PPy	-0.482	0.251	-0.283	0.334	4.74×10^{-7}
PPy@ TiO_2 layer	-0.665	0.291	0.275	0.492	6.72×10^{-7}
PEDOT	-0.631	0.16	0.156	0.344	4.77×10^{-7}
PEDOT @ TiO_2 layer	-0.740	0.21	0.351	0.531	7.46×10^{-7}

To evaluate the mechanism of the redox reactions of $\text{Co}^{2+}/\text{Co}^{3+}$ at the CE/electrolyte interface, the CVs of the PPy@TiO₂ and PEDOT@TiO₂ CEs at different scan rates were performed. The recorded CVs are presented in Supplementary Materials Figure S1a–d. As shown in Figure S1a,c a significant enhancement of the catalytic performance is indicated by the increasing J_{PC} . Figure S1b,d also revealed linear correlations between the J_{PC} , J_{OX} , and the square root of the scan rate, indicating that the redox reactions at the CE/electrolyte interfaces are diffusion-limited for the transport of $[\text{Co}(\text{bpy})_3]^{2+/3+}$ ions toward the CE, as described by the Randles–Sevcik theory (Equation (1)) [45]. This also suggests that the adsorption of $[\text{Co}(\text{bpy})_3]^{2+/3+}$ species is hardly affected by the redox reaction on the CE surface and that there are no specific interactions between the $\text{Co}^{2+}/\text{Co}^{3+}$ redox couple and the CE [46].

$$J_{\text{PC}} = Kn^{1.5}ACDn^{0.5}v^{0.5} \quad (1)$$

where K is the Boltzmann constant ($2.69 \times 10^5 \text{ J K}^{-1}$), A is the electrode surface area or the geometric surface area (cm^2), v is the scan rate (Vs^{-1}), n is the number of electrons participating in the redox event, C is the bulk concentration of the analyte (mol cm^{-3}), and D is the diffusion coefficient of the oxidized analyte ($\text{cm}^2 \text{ s}^{-1}$).

To further confirm the catalytic activity and interfacial charge-transfer properties of the $\text{Co}^{2+}/\text{Co}^{3+}$ redox couple at the CE in a practical electrolyte used in the DSSCs, Tafel polarization plots were recorded at a low scan rate (10 mVs^{-1}) using symmetrical electrochemical cells (CE/Electrolyte/CE). As shown in Figure 4b, the curve at a relatively moderate potential ($120 \text{ mV} < |V| < 400 \text{ mV}$) is assigned to the Tafel zone, where the exchange current density (J_0) can be determined by the intersection of the tangent line of the curve with the extension line of zero bias [27,47]. In the Tafel zone, J_0 is used as an indicator for the electrocatalytic activity of the CEs [44]. As shown in Equation (2), the J_0 value has an inverse relationship with the charge transfer resistance (R_{CT}).

$$J_0 = \frac{RT}{nFR_{\text{CT}}} \quad (2)$$

where R is the general gas constant ($8.3145 \text{ J mol}^{-1} \text{ K}^{-1}$), F is the Faraday constant ($26.801 \text{ Ah mol}^{-1}$), T is the Kelvin temperature, and n is the number of electrons involved in the redox reaction (here $n = 1$).

In the Tafel zone, the $\text{Log } J_0$ is linearly correlated with voltage, and the steep slope of the Tafel zone reveals a larger J_0 value, hence better electrocatalytic ability. As shown in Figure 4b and the estimated data in Table 1, the anodic and cathodic branches of the PPy CE show the smallest slope among all utilized CEs, while the slope of the PEDOT CE is better than that of the Pt CE. The larger slope indicates higher J_0 values and, thus, lower R_{CT} [27]. The slope of the $\text{log } J$ - V plots for all PPy@TiO₂ and PEDOT@TiO₂ CEs is larger, resulting in higher J_0 values and a lower R_{CT} . As presented in Table 1, PEDOT@TiO₂ CE displays the highest J_0 and lowest R_{CT} among all, which reveals the best catalytic activity toward the $\text{Co}^{2+}/\text{Co}^{3+}$ redox couple.

The limiting current density (J_{lim}) is another important parameter that can be estimated from the Tafel plot at the limiting diffusion zone at high potential ($|V| > 400 \text{ mV}$). The J_{lim} provides the maximum current that can flow from the DSSCs. The J_{lim} is usually obtained from the plateau current density in the high potential region of the Tafel plots [27]. Moreover, the diffusion coefficient (D_n) of the redox species is inversely dependent on the J_{lim} , as shown by Equation (3) [48].

$$D_n = \frac{L}{2nFC}J_{\text{lim}} \quad (3)$$

where L is the thickness of the diffusion layer (spacer), and C is the concentration of the oxidized species. Both n and F have the same meaning, as mentioned in Equation (2).

From the Tafel plots in Figure 3b and Table 1, the electrodeposited PPy and PEDOT CEs displayed almost the same J_{lim} values; however, the J_0 of PEDOT is much better.

After depositing the PPy and the PEDOT on the TiO₂ film, the estimated J_{lim} values of the obtained PPy@TiO₂ and PEDOT@TiO₂ CEs are much higher than those for the Pt CE, which reflect the higher D_n of Co³⁺ ions in the liquid electrolyte as described by Equation (3). As in Table 1, the estimated D_n of both PPy@TiO₂ and PEDOT@TiO₂ CEs are much better than that obtained by pure PPy, PEDOT CEs, and even higher than that for Pt CE. Overall, the higher J_o , J_{lim} , and D_n values of the PPy@TiO₂ and PEDOT@TiO₂ CEs indicate the positive influence of the TiO₂ film.

As the main function of CE in a DSSC device is to catalyze the redox reaction at the CE/electrolyte interface, it is important to understand the mechanism of these reactions. EIS was performed to measure the intrinsic interfacial charge transfer and charge transport kinetics at the CE/electrolyte interface [47]. The recorded Nyquist plots of the assembled symmetric cells are shown in Figure 5a,b and the fitted data are summarized in Table 2. It can be noticed that the cells with PPy, PPy@TiO₂, and Pt CEs showed two semicircles, while those with PEDOT, and PEDOT@TiO₂ CEs exhibited three semicircles, indicating the porous structure of these electrodes. The intersection of the first semicircle at high frequency with the real axis represents the Ohm serial resistance (R_s). From the first semicircle, the charge transfer resistance at the CE/electrolyte interface (R_{CT}) and the constant phase element (CPE) can be estimated [49]. The middle-frequency semi-circuit represents the diffusion impedance (Z_{diff}) of the redox species on a 3D layer, while the semi-circuit in the low-frequency region is from the diffusion resistance of the redox species in the electrolyte between the two electrodes, the Nernst diffusion impedance (Z_N) [44]. All assembled dummy cells have the same diffusion layer; thus, any decrease in Z_N can be attributed to the diffusion of the redox couple in the electrolyte [50]. As listed in Table 2, the R_s of the dummy cells with the electrodeposited pristine PPy and PEDOT CEs are slightly smaller than those with the PPy@TiO₂ and PEDOT@TiO₂ CEs, which reflects the influence of TiO₂ as a supporting layer for both polymers. The R_{CT} values of the cells with the electrodeposited PPy and PEDOT CE cells are 5.757 Ω and 5.655 Ω , respectively. Both are higher than that obtained by the cell with the Pt CE (5.618 Ω). This higher R_{CT} can be attributed to the compact structure of the pristine polymer layers, which reveals lower catalytic activity. Moreover, the dummy cells with PPy@TiO₂ and PEDOT@TiO₂ CEs give lower values due to the porous structure.

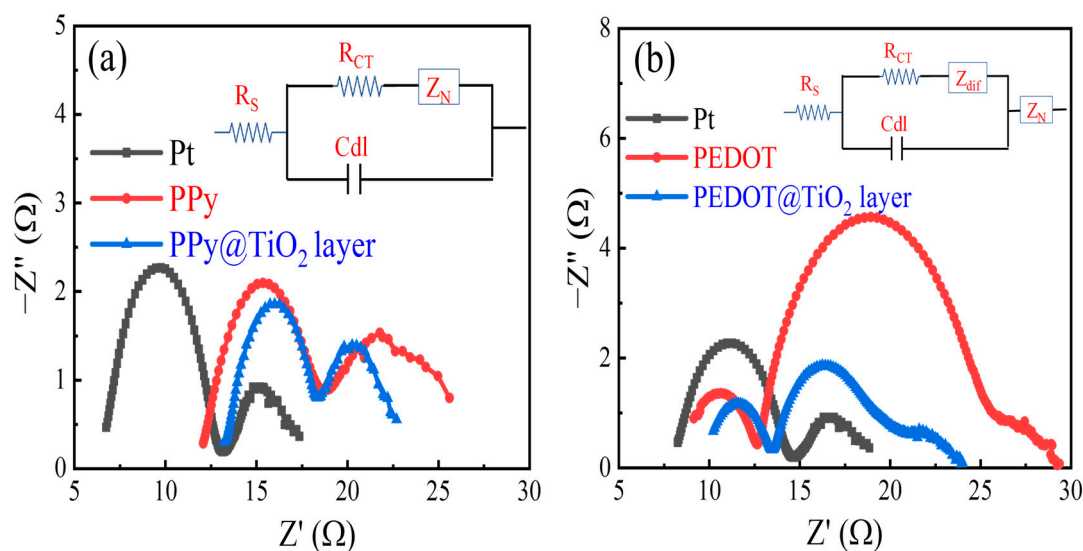


Figure 5. Nyquist plots of symmetric cells with (a) Pt, PPy, PEDOT, PPy@TiO₂, and (b) Pt, PEDOT@TiO₂ CEs (The inside upper is the equivalent circuit used for fitting the Nyquist plots).

Table 2. EIS parameters of the symmetric cells with various CEs and $[\text{Co}(\text{bpy})_3]^{2+/3+}$ redox couple.

CEs	R_S (Ω)	R_{CT} (Ω)	Z_{diff} (Ω)	Z_N (Ω)
Pt	7.868	5.618	—	3.278
PPy	12.350	5.757	—	7.811
PPy@TiO ₂ layer	13.430	5.007	—	5.605
PEDOT	7.443	5.655	13.059	6.554
PEDOT @TiO ₂ layer	8.000	4.457	6.792	5.115

The R_{CT} is used as an indicator for the electrocatalytic activity of the catalytic layer toward the redox reaction of the $\text{Co}^{2+}/\text{Co}^{3+}$ redox couple, the lower R_{CT} revealing higher catalytic activity of the CE toward the $\text{Co}^{2+}/\text{Co}^{3+}$ redox reaction and vice versa. The R_{CT} of the cell with PEDOT@TiO₂ CEs is the lowest (4.457 Ω), which implies the fastest charge transferability at the CE/electrolyte interface. These findings are in agreement with the Tafel and CV results, which support our claims that the catalytic performance can be boosted by depositing PPy and PEDOT onto a 3D hard template due to creating more active sites for the redox reaction [27]. As listed in Table 2, the Z_N of the cells based on the PPy CE and the PEDOT CE are 7.811 Ω , and 6.554 Ω , respectively. The Z_N of the assembled cells was reduced to 5.605 Ω and 5.115 Ω after depositing on TiO₂ film porous support, indicating a lower interfacial recombination rate [51]. The cell with the Pt CE had the smallest value (3.278 Ω) of all. The Nyquist plots of the cells based on PEDOT, and PEDOT@TiO₂ CEs showed three semi-circuits, indicating a porous structure. The estimated Z_{diff} of the cell with PEDOT CE (13.059 Ω) was reduced to 6.792 Ω after depositing on TiO₂, demonstrating the importance of TiO₂ as a supporting layer.

Sets of DSSCs were assembled and tested to assess the effectiveness of the prepared films as counter electrodes. The recorded photocurrent–voltage (J–V) curves are shown in Figure 6, and their related photovoltaic parameters are listed in Table 3. Among all devices, the DSSC with pristine PPy CE showed the lowest performance, with a PCE of 4.811%. This mainly arises from the low fill factor (FF = 69.041%) and low short circuit current ($J_{SC} = 8.611 \text{ mA cm}^{-2}$), which agree with the previous literature [27]. Moreover, the device with the PEDOT CE displayed better performance with a PCE of 6.141%, which is close to that achieved by the device with the Pt CE (6.065%). By utilizing PPy@TiO₂ and PEDOT@TiO₂ CEs, the assembled devices showed much better performances, in agreement with the previous electrochemical analysis. The PCE of the assembled devices with PPy@TiO₂ and PEDOT@TiO₂ CEs were 6.332% and 6.617%, respectively. The device with the PEDOT@TiO₂ CE displayed the highest performance among all.

Table 3. Photovoltaic parameters of DSSCs with various CEs and $[\text{Co}(\text{bpy})_3]^{2+/3+}$ redox couple.

CE	V_{OC} (V)	J_{SC} (mA cm^{-2})	FF (%)	PCE (%)
Pt	0.811	10.161	73.578	6.065
PPy	0.809	8.611	69.041	4.811
PPy@TiO ₂ layer	0.805	10.924	72.004	6.332
PEDOT	0.811	10.289	73.599	6.141
PEDOT @TiO ₂ layer	0.809	11.222	72.872	6.617

The J_{SC} is the distinguishing factor in the photovoltaic performance of the assembled devices, which can be assigned to the porous structures. Even though the V_{OC} of the assembled devices was nearly identical, the FF values varied. The device with the pristine PPy CE displayed the lowest FF (69.041%), which can be assigned to the higher series resistance resulting from the high compactness of the surface [52]. In the presence of the TiO₂ layer, a porous structure was formed, which significantly increased the FF to 72.004%. In the case of PEDOT-based devices, the insertion of TiO₂ results in lowering the FF, which

mainly can be attributed to reducing the conductivity. Carli et al. recently reported that a device with the electrodeposited PEDOT/Nafion CE had a PCE of 3.60% [35], which is significantly lower than the PCEs achieved by devices with a PPy@TiO₂ CE (6.33%) and PEDOT@TiO₂ CE (6.62%).

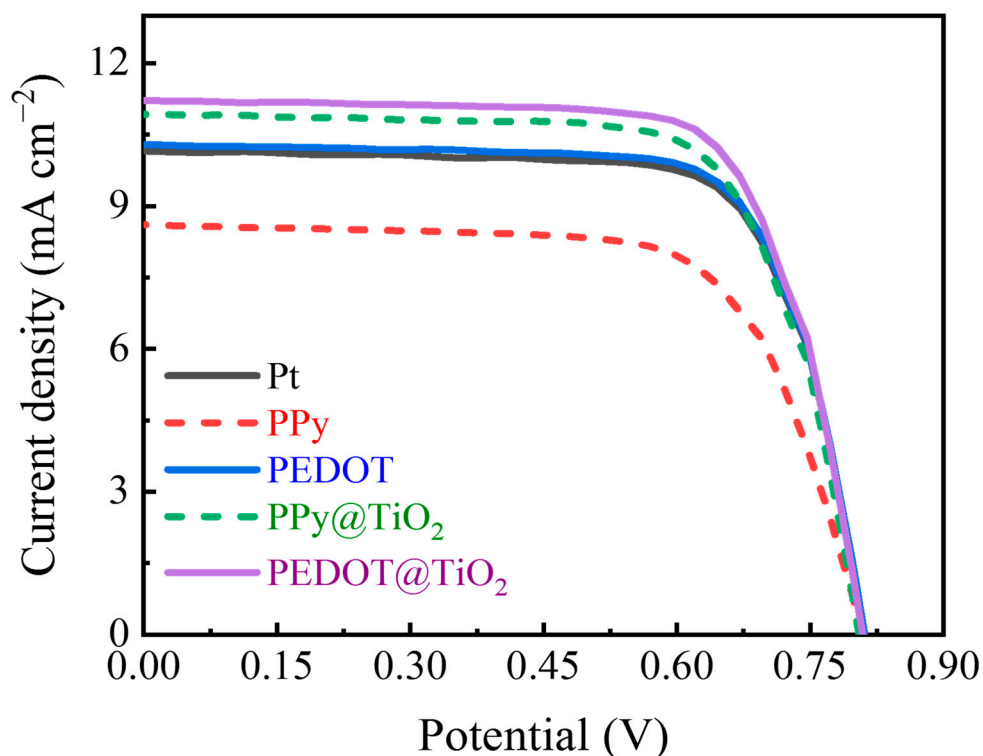


Figure 6. Photocurrent–voltage (J–V) curves of DSSCs with various counter electrodes.

3. Materials and Methods

3.1. Materials and Methods

Pyrrole, 3,4-ethylenedioxythiophene (EDOT), H₂SO₄ (98%), and sodium dodecyl sulphate (SDS) were purchased from Sigma Aldrich Co., Shanghai, China. 4-tert-butylpyridine (4-tBP), titanium di-isopropoxide bis (acetylacetonate) (TAA) [(CH₃)₂CHO]₂Ti (C₅H₇O₂)₂, 75 wt. % in isopropanol], bis (tri-fluoromethane) sulfonamide lithium salt (LiTFSI), hexachloroplatinic acid hexahydrate (H₂PtCl₆·6H₂O, 37.50% Pt basis), 2-methylimidazole (98%), tert-butyl alcohol (C₄H₁₀O, 97%), 2,2'-bipyridine, (C₁₀H₈N₂), nitrosonium tetrafluoroborate (NOBF₄, 95%), cobalt chloride (CoCl₂·6H₂O, 97%), platinum chloride (H₂PtCl₆), silver nitrate (AgNO₃, 99%), and MK-2 dye (C₅₈H₇₀N₂O₂S₄) from Sigma Aldrich Co. China. Anhydrous acetonitrile (CH₃CN, 99.80%) from Alfa Aesar, Beijing, China. Titanium dioxide paste (average particle size: 18, 30 nm, and 400 nm) and FTO conductive glass (2 mm thicknesses, square resistance 10–15 Ω·sq⁻¹) from OPV Tech Co., Ltd. Yingkou, China. Titanium (IV) tetrachloride (TiCl₄, 99.5–99.9%) from Sinopharm Chemical Reagent Beijing Co., Ltd., Beijing, China. De-ionized (DI) water was from an ultra-pure purifier (Ulu pure, Chengdu, China, resistivity ≥18.2 MΩ). All used reagents were of analytical purity and used as received from commercial sources without any further purification.

3.2. Working Electrodes and DSSCs

The working electrodes, or photoanodes, were prepared as previously described in our work [53]. Briefly, an FTO conducting glass plate was cut into pieces (1 cm × 1.5 cm) and washed with detergent, deionized (DI) water, and ethanol in a sequential process using an ultrasonic bath, followed by drying using a hot blower. A thin layer of TiO₂ (as a blocking layer) was formed on the conductive side of the pre-cleaned FTO species

via spray pyrolysis of 10% (*v/v*) solution of titanium isopropoxide bisacetyl acetonate in ethanol at 450 °C. The next layer (transparent layer) with ~6.0 μm thickness was formed by screen printing commercial TiO₂ paste (20 nm-sized). The printing process was repeated five times, followed by annealing at 120 °C for 10 min. A scattering layer with ~6.0 μm thickness was formed by printing a commercial TiO₂ paste (400 nm-sized) on top of a transparent layer and then heated at 120 °C for 10 min. The screen-printed TiO₂ films with 0.16 cm² active area were sintered at 500 °C for 30 min in a programmable system, followed by being treated in 20 mM TiCl₄ (aq) bath at 70 °C for 30 min. After being cooled to room temperature, the nanocrystalline TiO₂ electrode was washed with DI water and ethanol and fired again at 500 °C in the air for 30 min. Once cooled, the electrodes were bathed in a 0.3 mM solution of 0.3 mM MK-2 in absolute ethanol for 18 h at room temperature. The DSSCs were assembled by clipping the loaded dye TiO₂ photoanode with a CE using a 25 μm thick spacer (Solaronix SA, Aubonne, Switzerland) with inner of dimensions 5 × 6 mm. A liquid electrolyte of acetonitrile was injected into the gap between the clipping electrodes.

3.3. Preparation of PPy@TiO₂ and PEDOT@TiO₂ Counter Electrodes

The PPy@TiO₂ and PEDOT@TiO₂ CEs were prepared in two steps, as described below. First, a commercial TiO₂ paste (20 nm-sized) was screen printed onto cleaned FTO-glass substrates (10–15 Ω/□). The printed films were then annealed at 250 °C to remove the organic compounds, and finally subjected to further annealing at 500 °C for 30 min in the programmable system. The thickness of the printed TiO₂ layer was about 210–230 nm. The PPy and PEDOT were then electrodeposited on top of the TiO₂ using a three-electrode cell in which Pt foil served as the CE, an Ag/AgCl electrode served as the reference electrode, and FTO served as the working electrode. For PEDOT, the base electrodeposition solution consisted of 10 mM 3, 4-ethylenedioxythiophene (EDOT), 10 mM concentrated H₂SO₄, 100 mM LiTFSI, and 10 mM SDS in 20 mL DI water; the mixture was kept under an ultrasonic bath for 30 min. SDS, an anionic surfactant, was used as a dispersant, resulting in a homogeneous mixture of EDOT and water and lowering its oxidation potential to less than 1.0 V. Electrodeposition was performed at 1.1 V for 30 s; the electrodeposited electrodes were rinsed with absolute ethanol and dried in the atmosphere at room temperature.

For PPy, the base electrodeposition solution consisted of 10 mM of pyrrole, 10 mM concentrated H₂SO₄, 100 mM LiTFSI, and 10 mM SDS in 20 mL DI water; the mixture was treated using ultrasonication for 30 min. Electrodeposition was performed at 0.75 V for 30 s. The electrodeposited electrodes were rinsed with absolute ethanol and dried in the atmosphere at room temperature. The whole process utilized to prepare the electrodeposited electrodes is presented in Figure 7. For comparison, the pristine PEDOT PPy CEs were prepared using similar methods as the PPy@TiO₂ electrode. Furthermore, for comparison, Pt CEs were prepared by the thermal decomposition of 10 mM of H₂PtCl₆ in ethanol at 380 °C for 30 min [1].

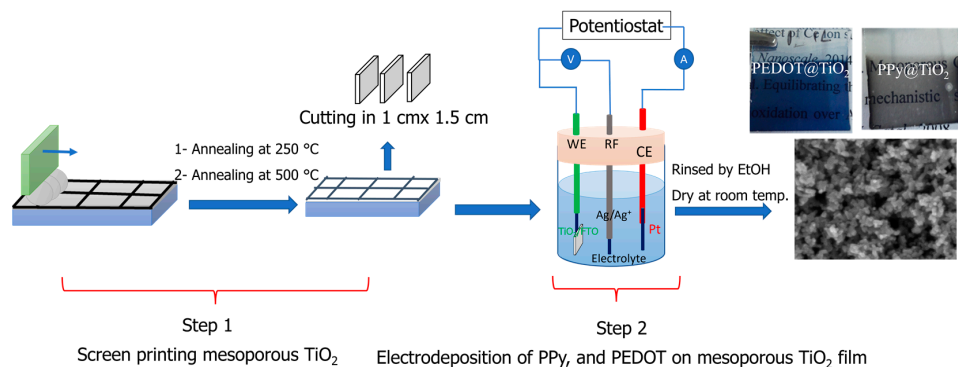


Figure 7. The Schematic representation for the preparation of PPy and PEDOT via electrodeposition process.

3.4. Characterization and Measurements

The surface morphologies were investigated by a field emission scanning electron microscope (SEM) JSM 7100F FESEM (Zeiss Ultra Plus) equipped with an energy dispersive spectrum (EDS) analyzer. The CV of the prepared CEs was performed by a conventional three-electrode electrochemical cell on the CHI760D electrochemical workstation. Ag/Ag⁺ served as the reference electrode, Pt coil as the counter electrode, and the as-prepared CEs as the working electrodes in nitrogen-purged anhydrous acetonitrile solution of 50 mM [Co(bpy)₃] (TFSI)₂, 50 mM [Co (bpy)₃] (TFSI)₃, and 100 mM LiTFSI supporting electrolyte for the [Co(bpy)₃]^{2+/3+} redox system. CV curves were recorded in the potential range from +0.6 V to −0.6 V at a 50 mVs^{−1} scan rate. Electrochemical impedance spectroscopy (EIS) of the symmetric cells was performed on an Ametek 1260 EIS instrument in a frequency range from 0.1 Hz to 100 KHz with 10 mV AC amplitude at zero bias potential under dark conditions. Z-view software was used to fit the impedance spectra by using a suitable equivalent circuit. The Tafel polarization test was performed on the electrochemical workstation with a 100 mVs^{−1} scan rate. The photocurrent density–voltage (J–V) curves of the DSSCs were recorded using the Newport solar simulator, USA (450 W Xe source) with a Keithley 2400 source meter, under irradiation (AM 1.5G, 0.1 Wcm^{−2} light radiation intensity). The light intensity was adjusted by a standard Si solar cell.

4. Conclusions

Here, PPy and PEDOT films were separately successfully electrodeposited on TiO₂ as a 3D porous template to be utilized as CEs for DSSCs based on the [Co(bpy)₃]^{2+/3+} redox couple. The morphological study indicated that the prepared films show a uniform porous structure, resulting in enhanced contact with the electrolyte and thus better electron transport. Electrochemical analysis demonstrated that the porous TiO₂ layer significantly enhanced the electrocatalytic activity of both PPy and PEDOT toward the [Co(bpy)₃]^{2+/3+} redox systems with much lower charge transfer resistance. This can be attributed to the synergistic effect between the high catalytic activity of PPy and PEDOT and the large surface area of the TiO₂ layer. The electrocatalytic performance of both PPy@TiO₂ and PEDOT@TiO₂ CEs outperformed the Pt CE with lower charge transfer resistances, and thus the assembled devices displayed higher power conversion efficiency. The PCE of the assembled DSSCs with the PPy@TiO₂ and PEDOT@TiO₂ CE are 6.33% and 6.62%, respectively; both are higher than that achieved with the Pt CE (6.07%), which highlights the potential use of these low-cost films for DSSCs with cobalt-based electrolytes.

Supplementary Materials: The following supporting information can be downloaded at: <https://www.mdpi.com/article/10.3390/inorganics10110213/s1>, The CV curves for both PPy@TiO₂ and PEDOT@TiO₂ CEs at different scan rates and their relationship between peak current density and the square root of scan rates are in supporting information, Figure S1.

Author Contributions: Formal analysis, A.S.A.A., X.Y. and W.X.; Funding acquisition, X.Z.; Methodology, A.S.A.A.; Software, X.Y.; Supervision, X.Z. and M.A.; Validation, M.A.; Visualization, W.X.; Writing—original draft, A.S.A.A.; Writing—review & editing, W.X. All authors have read and agreed to the published version of the manuscript.

Funding: This research received no external funding.

Institutional Review Board Statement: Not applicable.

Informed Consent Statement: Not applicable.

Data Availability Statement: Not applicable.

Acknowledgments: The authors gratefully acknowledge W. Xiang for providing Co electrolyte. They also wish to thank Mohamed Taher for providing pyrrole and sodium dodecyl sulphate (SDS), as well as helping with the electropolymerizing technique.

Conflicts of Interest: The authors declare no conflict of interest.

References

1. Hagfeldt, A.; Boschloo, G.; Sun, L.; Kloo, L.; Pettersson, H. Dye-Sensitized Solar Cells. *Chem. Rev.* **2010**, *110*, 6595–6663. [[CrossRef](#)] [[PubMed](#)]
2. Grätzel, M. Photoelectrochemical cells. *Nature* **2001**, *414*, 338–344. [[CrossRef](#)] [[PubMed](#)]
3. O'Regan, B.; Grätzel, M. A low-cost, high-efficiency solar cell based on dye-sensitized colloidal TiO₂ films. *Nature* **1991**, *353*, 737–740. [[CrossRef](#)]
4. Ito, S.; Chen, P.; Comte, P.; Nazeeruddin, M.K.; Liska, P.; Péchy, P.; Grätzel, M. Fabrication of screen-printing pastes from TiO₂ powders for dye-sensitized solar cells. *Prog. Photovolt. Res. Appl.* **2007**, *15*, 603–612. [[CrossRef](#)]
5. Mathew, S.; Yella, A.; Gao, P.; Humphry-Baker, R.; Curchod, B.F.; Ashari-Astani, N.; Tavernelli, I.; Rothlisberger, U.; Nazeeruddin, M.K.; Grätzel, M. Dye-sensitized solar cells with 13% efficiency achieved through the molecular engineering of porphyrin sensitizers. *Nat. Chem.* **2014**, *6*, 242–247. [[CrossRef](#)] [[PubMed](#)]
6. Zhang, L.; Yang, X.; Wang, W.; Gurzadyan, G.G.; Li, J.; Li, X.; An, J.; Yu, Z.; Wang, H.; Cai, B.; et al. 13.6% Efficient Organic Dye-Sensitized Solar Cells by Minimizing Energy Losses of the Excited State. *ACS Energy Lett.* **2019**, *4*, 943–951. [[CrossRef](#)]
7. Murakami, T.N.; Grätzel, M. Counter electrodes for DSC: Application of functional materials as catalysts. *Inorg. Chim. Acta* **2008**, *361*, 572–580. [[CrossRef](#)]
8. Wu, J.; Lan, Z.; Lin, J.; Huang, M.; Huang, Y.; Fan, L.; Luo, G.; Lin, Y.; Xie, Y.; Wei, Y. Counter electrodes in dye-sensitized solar cells. *Chem. Soc. Rev.* **2017**, *46*, 5975–6023. [[CrossRef](#)]
9. Thomas, S.; Deepak, T.G.; Anjusree, G.S.; Arun, T.A.; Nair, S.V.; Nair, A.S. A review on counter electrode materials in dye-sensitized solar cells. *J. Mater. Chem. A* **2014**, *2*, 4474–4490. [[CrossRef](#)]
10. Green, M.A.; Emery, K.; Hishikawa, Y.; Warta, W.; Dunlop, E.D. Solar cell efficiency tables (version 47). *Prog. Photovolt. Res. Appl.* **2016**, *24*, 3–11. [[CrossRef](#)]
11. Thogiti, S.; Park, J.Y.; Thanh Thuy, C.T.; Lee, D.K.; Min, B.-K.; Yun, H.J.; Kim, J.H. High-Performance Dye-Sensitized Solar Cells through Graded Electron Transport in Band-Engineered W-TiO₂ Cascade Layer. *ACS Sustain. Chem. Eng.* **2018**, *6*, 13025–13034. [[CrossRef](#)]
12. Gurulakshmi, M.; Meenakshamma, A.; Susmitha, K.; Venkata Subbaiah, Y.P.; Mitty, R. Enhanced Performance of Dye-Sensitized Solar Cells (DSSCs) Based on MoS₂/Single-Walled Carbon Nanohorns Electrochemically Deposited on Bilayer Counter Electrodes. *Chem. Plus Chem.* **2020**, *85*, 2599–2605. [[CrossRef](#)] [[PubMed](#)]
13. Wang, M.; Grätzel, C.; Zakeeruddin, S.M.; Grätzel, M. Recent developments in redox electrolytes for dye-sensitized solar cells. *Energy Environ. Sci.* **2012**, *5*, 9394–9405. [[CrossRef](#)]
14. Spokoyny, A.M.; Li, T.C.; Farha, O.K.; Machan, C.W.; She, C.; Stern, C.L.; Marks, T.J.; Hupp, J.T.; Mirkin, C.A. Electronic Tuning of Nickel-Based Bis(dicarbollide) Redox Shuttles in Dye-Sensitized Solar Cells. *Angew. Chem. Int. Ed.* **2010**, *49*, 5339–5343. [[CrossRef](#)] [[PubMed](#)]
15. Saygili, Y.; Söderberg, M.; Pellet, N.; Giordano, F.; Cao, Y.; Muñoz-García, A.B.; Zakeeruddin, S.M.; Vlachopoulos, N.; Pavone, M.; Boschloo, G.; et al. Copper Bipyridyl Redox Mediators for Dye-Sensitized Solar Cells with High Photovoltage. *J. Am. Chem. Soc.* **2016**, *138*, 15087–15096. [[CrossRef](#)]
16. Wang, M.; Chamberland, N.; Breau, L.; Moser, J.E.; Humphry-Baker, R.; Marsan, B.; Zakeeruddin, S.M.; Grätzel, M. An organic redox electrolyte to rival triiodide/iodide in dye-sensitized solar cells. *Nat. Chem.* **2010**, *2*, 385–389. [[CrossRef](#)]
17. Daeneke, T.; Kwon, T.H.; Holmes, A.B.; Duffy, N.W.; Bach, U.; Spiccia, L. High-efficiency dye-sensitized solar cells with ferrocene-based electrolytes. *Nat. Chem.* **2011**, *3*, 211–215. [[CrossRef](#)]
18. Bella, F.; Galliano, S.; Gerbaldi, C.; Viscardi, G. Cobalt-Based Electrolytes for Dye-Sensitized Solar Cells: Recent Advances towards Stable Devices. *Energies* **2016**, *9*, 384. [[CrossRef](#)]
19. Nusbaumer, H.; Moser, J.-E.; Zakeeruddin, S.M.; Nazeeruddin, M.K.; Grätzel, M. CoII(dbbip)₂²⁺ Complex Rivals Triiodide/Iodide Redox Mediator in Dye-Sensitized Photovoltaic Cells. *J. Phys. Chem. B* **2001**, *105*, 10461–10464. [[CrossRef](#)]
20. Klahr, B.M.; Hamann, T.W. Performance Enhancement and Limitations of Cobalt Bipyridyl Redox Shuttles in Dye-Sensitized Solar Cells. *J. Phys. Chem. C* **2009**, *113*, 14040–14045. [[CrossRef](#)]
21. Tsao, H.N.; Yi, C.; Moehl, T.; Yum, J.H.; Zakeeruddin, S.M.; Nazeeruddin, M.K.; Grätzel, M. Cyclopentadithiophene bridged donor-acceptor dyes achieve high power conversion efficiencies in dye-sensitized solar cells based on the tris-cobalt bipyridine redox couple. *Chem. Sus. Chem.* **2011**, *4*, 591–594. [[CrossRef](#)] [[PubMed](#)]
22. Sapp, S.A.; Elliott, C.M.; Contado, C.; Caramori, S.; Bignozzi, C.A. Substituted Polypyridine Complexes of Cobalt(II/III) as Efficient Electron-Transfer Mediators in Dye-Sensitized Solar Cells. *J. Am. Chem. Soc.* **2002**, *124*, 11215–11222. [[CrossRef](#)] [[PubMed](#)]
23. Feldt, S.M.; Gibson, E.A.; Gabrielsson, E.; Sun, L.; Boschloo, G.; Hagfeldt, A. Design of Organic Dyes and Cobalt Polypyridine Redox Mediators for High-Efficiency Dye-Sensitized Solar Cells. *J. Am. Chem. Soc.* **2010**, *132*, 16714–16724. [[CrossRef](#)] [[PubMed](#)]
24. Yella, A.; Lee, H.W.; Tsao, H.N.; Yi, C.; Chandiran, A.K.; Nazeeruddin, M.K.; Diau, E.W.; Yeh, C.Y.; Zakeeruddin, S.M.; Grätzel, M. Porphyrin-sensitized solar cells with cobalt (II/III)-based redox electrolyte exceed 12 percent efficiency. *Science* **2011**, *334*, 629–634. [[CrossRef](#)]
25. Baptyayev, B.; Mustazheb, D.; Balanay, M.P. Binary transition metal sulfides as an economical Pt-free counter electrodes for dye-sensitized solar cells. *Mater. Today Proc.* **2020**, *25*, 24–27. [[CrossRef](#)]

26. Hattori, S.; Wada, Y.; Yanagida, S.; Fukuzumi, S. Blue Copper Model Complexes with Distorted Tetragonal Geometry Acting as Effective Electron-Transfer Mediators in Dye-Sensitized Solar Cells. *J. Am. Chem. Soc.* **2005**, *127*, 9648–9654. [[CrossRef](#)]
27. He, J.; Pringle, J.M.; Cheng, Y.-B. Titanium Carbide and Titanium Nitride-Based Nanocomposites as Efficient Catalysts for the $\text{Co}^{2+}/\text{Co}^{3+}$ Redox Couple in Dye-Sensitized Solar Cells. *J. Phys. Chem. C* **2014**, *118*, 16818–16824. [[CrossRef](#)]
28. Carli, S.; Busatto, E.; Caramori, S.; Boaretto, R.; Argazzi, R.; Timpson, C.J.; Bignozzi, C.A. Comparative Evaluation of Catalytic Counter Electrodes for Co(III)/(II) Electron Shuttles in Regenerative Photoelectrochemical Cells. *J. Phys. Chem. C* **2013**, *117*, 5142–5153. [[CrossRef](#)]
29. Lu, S.; Yang, H.; Li, F.; Wang, Y.; Chen, S.; Yang, G.; Liu, Y.; Zhang, X. Element substitution of kesterite $\text{Cu}_2\text{ZnSnS}_4$ for efficient counter electrode of dye-sensitized solar cells. *Sci. Rep.* **2018**, *8*, 8714. [[CrossRef](#)]
30. Huang, Y.-J.; Chen, H.-T.; Ann, S.-B.; Li, C.-T.; Lin, J.T.; Lee, C.-P.; Ho, K.-C. Hierarchical urchin-like $\text{CoSe}_2/\text{CoSeO}_3$ electrocatalysts for dye-sensitized solar cells: Up to 19% PCE under dim light illumination. *J. Mater. Chem. A* **2019**, *7*, 26089–26097. [[CrossRef](#)]
31. Pang, B.; Zhang, M.; Zhou, C.; Dong, H.; Ma, S.; Shi, Y.; Sun, Q.; Li, F.; Yu, L.; Dong, L. Nitrogen-Doped Carbon Nano-Onions Decorated on Graphene Network: A Novel All-Carbon Composite Counter Electrode for Dye-Sensitized Solar Cell with a 10.28% Power Conversion Efficiency. *Sol. RRL* **2020**, *4*, 2000263. [[CrossRef](#)]
32. Ahmed, A.S.A.; Xiang, W.; Abdelmotalleib, M.; Zhao, X. Efficient NiO Impregnated Walnut Shell-Derived Carbon for Dye-Sensitized Solar Cells. *ACS Appl. Electron. Mater.* **2022**, *4*, 1063–1071. [[CrossRef](#)]
33. Ahmed, A.S.A.; Xiang, W.; Gu, A.; Hu, X.; Saana, I.A.; Zhao, X. Carbon black/silicon nitride nanocomposites as high-efficiency counter electrodes for dye-sensitized solar cells. *New J. Chem.* **2018**, *42*, 11715–11723. [[CrossRef](#)]
34. Abdelaal, S.A.A.; Wanchun, X.; Fatma, S.M.H.; Xiujian, Z. Screen-printed carbon black/ SiO_2 composite counter electrodes for dye-sensitized solar cells. *Sol. Energy* **2021**, *230*, 902–911. [[CrossRef](#)]
35. Marchini, E.; Orlandi, M.; Bazzanella, N.; Boaretto, R.; Cristino, V.; Miotello, A.; Caramori, S.; Carli, S. Electrodeposited PEDOT/Nafion as Catalytic Counter Electrodes for Cobalt and Copper Bipyridyl Redox Mediators in Dye-Sensitized Solar Cells. *ACS Omega* **2022**, *7*, 29181–29194. [[CrossRef](#)] [[PubMed](#)]
36. Kavan, L.; Yum, J.H.; Grätzel, M. Graphene nanoplatelets outperforming platinum as the electrocatalyst in co-bipyridine-mediated dye-sensitized solar cells. *Nano Lett.* **2011**, *11*, 5501–5506. [[CrossRef](#)] [[PubMed](#)]
37. Ju, M.J.; Kim, J.C.; Choi, H.-J.; Choi, I.T.; Kim, S.G.; Lim, K.; Ko, J.; Lee, J.-J.; Jeon, I.-Y.; Baek, J.-B.; et al. N-Doped Graphene Nanoplatelets as Superior Metal-Free Counter Electrodes for Organic Dye-Sensitized Solar Cells. *ACS Nano* **2013**, *7*, 5243–5250. [[CrossRef](#)]
38. Liu, I.P.; Hou, Y.-C.; Li, C.-W.; Lee, Y.-L. Highly electrocatalytic counter electrodes based on carbon black for cobalt(iii)/(ii)-mediated dye-sensitized solar cells. *J. Mater. Chem. A* **2017**, *5*, 240–249. [[CrossRef](#)]
39. Li, Y.; Feng, Q.; Wang, H.; Zhou, G.; Wang, Z.-S. Reduced graphene oxide– Ta_3N_5 composite: A potential cathode for efficient $\text{Co}(\text{bpy})_3^{3+/2+}$ mediated dye-sensitized solar cells. *J. Mater. Chem. A* **2013**, *1*, 6342–6349. [[CrossRef](#)]
40. Marchini, E.; Caramori, S.; Bignozzi, C.A.; Carli, S. On the Use of PEDOT as a Catalytic Counter Electrode Material in Dye-Sensitized Solar Cells. *Appl. Sci.* **2021**, *11*, 3795. [[CrossRef](#)]
41. Park, B.-w.; Pazoki, M.; Aitola, K.; Jeong, S.; Johansson, E.M.J.; Hagfeldt, A.; Boschloo, G. Understanding Interfacial Charge Transfer between Metallic PEDOT Counter Electrodes and a Cobalt Redox Shuttle in Dye-Sensitized Solar Cells. *ACS Appl. Mater. Interfaces* **2014**, *6*, 2074–2079. [[CrossRef](#)] [[PubMed](#)]
42. Reinmuth, W.H. Theory of Stationary Electrode Polarography. *Anal. Chem.* **1961**, *33*, 1793–1794. [[CrossRef](#)]
43. Peng, S.; Tian, L.; Liang, J.; Mhaisalkar, S.G.; Ramakrishna, S. Polypyrrole nanorod networks/carbon nanoparticles composite counter electrodes for high-efficiency dye-sensitized solar cells. *ACS Appl. Mater. Interfaces* **2012**, *4*, 397–404. [[CrossRef](#)] [[PubMed](#)]
44. Wu, M.; Lin, X.; Wang, Y.; Wang, L.; Guo, W.; Qi, D.; Peng, X.; Hagfeldt, A.; Grätzel, M.; Ma, T. Economical Pt-Free Catalysts for Counter Electrodes of Dye-Sensitized Solar Cells. *J. Am. Chem. Soc.* **2012**, *134*, 3419–3428. [[CrossRef](#)]
45. Huang, S.; He, Q.; Chen, W.; Zai, J.; Qiao, Q.; Qian, X. 3D hierarchical FeSe_2 microspheres: Controlled synthesis and applications in dye-sensitized solar cells. *Nano Energy* **2015**, *15*, 205–215. [[CrossRef](#)]
46. Afshari, M.; Dinari, M.; Momeni, M.M. Ultrasonic irradiation preparation of graphitic- C_3N_4 /polyaniline nanocomposites as counter electrodes for dye-sensitized solar cells. *Ultrason. Sonochem.* **2018**, *42*, 631–639. [[CrossRef](#)]
47. He, Q.; Huang, S.; Wang, C.; Qiao, Q.; Liang, N.; Xu, M.; Chen, W.; Zai, J.; Qian, X. The role of Mott-Schottky heterojunctions in $\text{Ag-Ag}_8\text{SnS}_6$ as counter electrodes in dye-sensitized solar cells. *ChemSusChem* **2015**, *8*, 817–820. [[CrossRef](#)]
48. He, B.; Tang, Q.; Wang, M.; Chen, H.; Yuan, S. Robust Polyaniline–Graphene Complex Counter Electrodes For Efficient Dye-Sensitized Solar Cells. *ACS Appl. Mater. Interfaces* **2014**, *6*, 8230–8236. [[CrossRef](#)]
49. Kavan, L.; Yum, J.H.; Graetzel, M. Optically transparent cathode for Co(III/II) mediated dye-sensitized solar cells based on graphene oxide. *ACS Appl. Mater. Interfaces* **2012**, *4*, 6999–7006. [[CrossRef](#)]
50. Wu, M.; Wang, Y.; Lin, X.; Guo, W.; Wu, K.; Lin, Y.-N.; Guo, H.; Ma, T. TiC/Pt composite catalyst as counter electrode for dye-sensitized solar cells with long-term stability and high efficiency. *J. Mater. Chem. A* **2013**, *1*, 9672–9679. [[CrossRef](#)]
51. Huang, S.; Zai, J.; Ma, D.; Hu, Z.; He, Q.; Wu, M.; Chen, D.; Chen, Z.; Qian, X. Improving the catalytic performance of Ni_3S_4 -PtCo heteronanorods via Mott-Schottky effect toward the reduction of iodine couples in dye-sensitized solar cells. *Electrochim. Acta* **2017**, *241*, 89–97. [[CrossRef](#)]

-
52. Aftabuzzaman, M.; Sarker, S.; Lu, C.; Kim, H.K. In-depth understanding of the energy loss and efficiency limit of dye-sensitized solar cells under outdoor and indoor conditions. *J. Mater. Chem. A* **2021**, *9*, 24830–24848. [[CrossRef](#)]
 53. Ahmed, A.S.A.; Xiang, W.; Shui, F.; Li, B.; Younes, H.H.A.; Amiin, I.S.; Zhao, X. MoS₂/ZIF-8 derived nitrogen doped carbon (NC)-PEDOT: PSS as optically transparent counter electrode for dye-sensitized solar cells. *Sol. Energy* **2021**, *218*, 117–128. [[CrossRef](#)]